0026-895X/90/010072-12$02.00/0

MOLECULAR PHARMACOLOGY, 38:72-83

Analysis of Agonist-Antagonist Interactions at A_1 Adenosine Receptors

EDWARD LEUNG, KENNETH A. JACOBSON, and RICHARD D. GREEN

Department of Pharmacology, College of Medicine, University of Illinois at Chicago, Chicago, Illinois 60680 (E.L., R.D.G.), and Laboratory of Chemistry, National Institute of Diabetes, Digestive and Kidney Diseases, National Institutes of Health, Bethesda, Maryland 20892 (K.A.J.)

Received September 5, 1989; Accepted April 19, 1990

SUMMARY

Previous work from our laboratory using sucrose gradient centrifugation and the antagonist radioligand [^{3}H]xanthine amine congener led us to propose that A_1 adenosine receptors are coupled to a GTP-binding protein (G protein) in the absence of an agonist and that adenosine receptor antagonists bind to free uncoupled receptors with high affinity and coupled receptors with low affinity and cause a destabilization of receptor-G protein complexes [*Mol. Pharmacol.* **36**:412–419 (1989)]. Because agonists form high affinity ternary complexes composed of the agonist, receptor, and G protein, this hypothesis would imply that interactions between adenosine receptor agonists and antagonists, while competitive, would appear to be "noncompetitive" in nature. Interactions between unlabeled and radiolabeled A_1 receptor agonist and antagonist ligands have been investigated using bovine cerebral cortical membranes to further probe this point. The availability of both ^{3}H- and ^{125}I-radioligands allowed us to use both single- and dual-isotope experimental designs. Radioligand antagonist-agonist competition curves along with saturation analyses using filtration and centrifugation to isolate bound radioligand suggested that agonists bind to two sites or receptor states with high affinity and to one site with low affinity. Agonist radioligand saturation curves with or without unlabeled antagonist suggested that antagonists do not bind to all states of the receptor with equal affinity. The computer program EQUIL was used to define models capable of simultaneously fitting all parts of complex experiments in which ^{125}I-N^6-aminobenzyladenosine saturation isotherms with or without 8-cyclopentyl-1,3-dipropylxanthine ([^{3}H]CPX) and a saturation isotherm of [^{3}H]CPX were performed. The data were not compatible with two-independent site models or with ternary complex models involving one receptor and one G protein. The data were fit by a model involving one receptor and two G proteins and by a model involving two receptors and one G protein. Both models suggest that 1) a high percentage of the receptor(s) is coupled to a G protein in the absence of an agonist and 2) agonists stabilize whereas antagonists destabilize precoupled receptor-G protein complexes. Because of this, competitive interactions between A_1 agonists and antagonists appear noncompetitive in nature.

A_1-Adenosine receptors are widely distributed throughout the brain and have been extensively studied using both ligand binding (1) and radioligand-autoradiography (2) methodologies. Early studies used the agonist radioligands [^{3}H]CHA (3), (*R*)-[^{3}H]PIA (4), and [^{3}H]2-chloroadenosine (5) and the antagonist radioligand [^{3}H]1,3-diethyl-8-phenylxanthine (3). Other agonist radioligands such as [^{3}H]N^6-cyclopentyladenosine (6), ^{125}I-N^6-hydroxyphenylisopropyladenosine (7), and ^{125}I-ABA (8) were subsequently introduced. Recently, three new alkylxanthine antagonist radioligands, [^{3}H]XAC (9), [^{3}H]CPX (10, 11), and ^{125}I-BW-A844U (12) were introduced and shown to be markedly superior to [^{3}H]1,3-diethyl-8-phenylxanthine. Although it is not clear whether the receptors characterized by ligand binding studies are those that mediate the inhibition of adenylate cyclase (13) and/or the activation of K^+ channels (14), the latter two responses are classified as A_1 receptor-mediated responses. Both the physiological/biochemical responses and ligand binding are sensitive to guanine nucleotides, suggesting that a G protein(s) is involved (13, 14).

As with other receptors that couple to G proteins, the number of sites detected with the antagonist radioligands (B_{max} values) is usually greater than the corresponding B_{max} values for agonist radioligands (10, 13). Although it is clear that agonist binding is sensitive to guanine nucleotides and that multiple affinity states of agonist binding exist (10–13), the existence of more than one affinity state for antagonist binding is controversial. Some authors (13, 15, 16) but not others (17) have found that antagonist radioligand binding is increased by guanine nucleotides. We previously suggested that antagonists bind to free A_1 receptors with high affinity but to A_1 receptor-G protein complexes with lower affinity, whereas the opposite pertains for agonists (18).

These studies were supported by a grant from the National Science Foundation (BNS-8719594). E.L. was supported by a fellowship from the Chicago Heart Association.

ABBREVIATIONS: ABA, N^6-aminobenzyladenosine; CHA, N^6-cyclohexyladenosine; CPX, 8-cyclopentyl-1,3-dipropylxanthine; Gpp(NH)p, 5′-guanylylimidodiphosphate; NEM, *N*-ethylmaleimide; PIA, N^6-phenylisopropyladenosine; XAC, xanthine amine congener; G protein, GTP-binding protein.

A seemingly unrelated but, in fact, very germane observation is that agonists retain their ability to form high affinity complexes with A_1 receptors after solubilization (19, 20). This is contrary to the situation with β-adrenergic (21) and α_2-adrenergic receptors (22, 23). One possible explanation is that A_1 receptor-G protein complexes exist in the membrane in the absence of an agonist and that this complex is stable to solubilization. We recently reported sucrose gradient centrifugation studies with the agonist ligand ^{125}I-ABA and the antagonist radioligand [^{3}H]XAC that gave direct physical evidence for this hypothesis (18). Furthermore, these studies suggested that antagonists bind preferentially to free A_1 receptors and cause a destabilization of precoupled receptor-G protein complexes. If true, this has important consequences, the most obvious being that the characteristics of the interactions between agonists and antagonists would not appear competitive. The work reported herein addresses the mechanisms of A_1 agonist-antagonist interactions in detail, using preparations of bovine brain.

Experimental Procedures

Preparation of membranes. Brains from freshly killed calves were obtained at a local abattoir. Ten to fifteen grams of cerebral cortex were minced and homogenized in a buffer containing a mixture of protease inhibitors, and a P_2 fraction was prepared as previously described (18). Aliquots of the membrane preparations were stored under liquid nitrogen until use.

Radioligand binding. Samples containing 20 mM Tris·HCl, pH 7.5 at 25°, 4 or 10 mM $MgSO_4$, 1 mM EDTA, a mixture of protease inhibitors (24), 0.2 units/ml adenosine deaminase, radioligand, and membrane preparation were incubated at 37° for a time to ensure equilibrium (90–120 min unless otherwise specified), at which time bound and free radioligand were separated using polyethylenimine-soaked GF/A filters and a Brandel filtration apparatus, as described previously (24). In a limited number of experiments, bound and free radioligand were separated by centrifugation in 1.5-ml Microfuge tubes. After centrifugation, the supernatants were aspirated and the pellets were isolated by cutting off the tips of the microfuge tubes. Samples containing ^{125}I were counted directly in a γ-counter; samples containing ^{3}H were solubilized using TS-1 (RPI, Mount Prospect, IL) before being counted in a liquid scintillation counter. Incubation volumes and amounts of membrane preparation were adjusted so that amounts of radioactivity bound could be easily quantified without binding of a significant amount of the total radioligand (generally 50–100 μl and 10–20 μg of protein for ^{125}I-ABA and 500 μl and 20–50 μg of protein for the ^{3}H-radioligands). In general, nonspecific binding of agonist radioligands was determined using 100 μM (*R*)-PIA, whereas 5 mM theophylline was used to determine the nonspecific binding of the antagonist radioligands. This was done because high concentrations ($\gg K_d$) of agonist radioligands were not completely displaced by 5 mM theophylline; conversely, high concentrations of antagonist radioligands were not completely displaced by 100 μM (*R*)-PIA. Samples containing ^{125}I were counted in a γ-counter (LKB model 1272) at 75% efficiency; samples containing ^{3}H were counted in a liquid scintillation counter at 45% efficiency (Beckman model LS3801). ^{125}I and ^{3}H in samples containing both isotopes were counted as previously described (18). The specific activity of the ^{125}I-ABA used in dual-isotope experiments was adjusted to 250–300 Ci/mmol, as previously described (24).

Sucrose gradient centrifugation. Membranes were incubated (90 min, 37°) with or without radioligand (^{125}I-ABA or [^{3}H]CPX), pelleted, solubilized with digitonin, and run on 12.5-ml sucrose density gradients (5–20%), as detailed previously (18). Gradients were fractionated and bound radioactivity was collected by filtration over polyethylenimine-soaked GF/B glass fiber filters (25).

Data analysis. As indicated in the text, data were analyzed by least squares linear regression (linear Scatchard plots, rate plots), nonlinear regression using the program LIGAND (26) (linear and nonlinear Scatchard plots and inhibition curves), and a newly written program entitled EQUIL (27).

Materials. ^{125}I-ABA was synthesized and purified as previously described (24). A theoretical specific activity of 2200 Ci/mmol was assumed. [^{3}H]XAC (130–157 Ci/mmol) and (*R*)-[^{3}H]PIA (49.9 Ci/mmol) were from DuPont-NEN; [^{3}H]CPX (95–103 Ci/mmol) and ACS scintillation cocktail were from Amersham. I-ABA was kindly provided by Dr. Joel Linden (University of Virginia, Charlottesville, VA). All other chemicals were from Sigma Chemical Co.

Results

Kinetics of radioligand binding. Fig. 1A shows semilogarithmic plots of the association or on-rate of binding of the agonist radioligand (*R*)-[^{3}H]PIA at different ligand concentrations (*L*). The association at all ligand concentrations was monophasic, with the slope equal to the k_{obs}. A secondary plot of k_{obs} versus *L*, if linear, has a slope of k_{+1} and an intercept of k_{-1} (28). The secondary plot of these data was linear and is shown in Fig. 1A, *inset* (k_{+1} = 0.1648 nM^{-1} min^{-1}, k_{-1} = 0.0192 min^{-1}, and $k_{-1}/k_{+1} = K_d$ = 0.12 nM). A similar experiment for a second agonist radioligand, ^{125}I-ABA, is summarized graphically in Fig. 1B (k_{+1} = 0.1221 nM^{-1} min^{-1}, k_{-1} = 0.0209 min^{-1}, and K_d = 0.17 nM). In both cases, the k_{-1} determined from the secondary plots agreed well with those determined directly by dilution or by the addition of unlabeled agonist ligand (data not shown).

Fig. 1C summarizes a similar experiment with the antagonist radioligand [^{3}H]CPX. As with both (*R*)-[^{3}H]PIA and ^{125}I-ABA, the on-rates were monophasic and the secondary plot (Fig. 1C, *inset*) was linear, giving k_{+1} = 0.8020 nM^{-1} min^{-1}, k_{-1} = 0.0672 min^{-1}, and K_d = 0.084 nM. Again, the k_{-1} determined from the secondary plot agreed well with that determined by dilution (data not shown). Experiments shown in Fig. 1 are representative of two experiments of each type, which, in all cases, gave similar results. Kinetic experiments with the antagonist [^{3}H]XAC gave more complicated results, in that the association rate in the absence of added guanine nucleotide was biphasic, whereas the association rate in the presence of Gpp(NH)p was monophasic (Fig. 2A). Similar results for the binding of [^{3}H]XAC to A_1 receptors in rat adipocyte membranes were reported by Ramkumar and Stiles (15). The dissociation of [^{3}H]XAC [minus Gpp(NH)p] was monophasic, with a k_{-1} of 0.0415 ± 0.02 min^{-1} ($t_{1/2}$ = 16.7 ± 0.8 min, six experiments). Fig. 2B summarizes an experiment in which NEM pretreatment was used to disrupt A_1 receptor-G protein interactions (13). The on-rates of [^{3}H]XAC binding were monophasic; the secondary plot (Fig. 2B, *inset*) gave k_{+1} = 0.56 nM^{-1} min^{-1}, k_{-1} = 0.086 min^{-1}, and K_d = 0.15 nM. However, it should be noted that this experiment did not always give satisfactory results. Because antagonist radioligand binding (37°) to receptors in untreated membranes in the presence of Gpp(NH)p or to receptors in NEM-treated membranes at 37° exhibits varying degrees of stability with time (binding increases and sometimes then decreases with time),[1] the variability in the success of these experiments probably reflects a relative instability of free receptors.

Equilibrium binding of (*R*)-[^{3}H]PIA, [^{3}H]XAC, and [^{3}H]CPX. Saturation isotherms for the binding of (*R*)-[^{3}H]PIA, [^{3}H]XAC, and [^{3}H]CPX were determined in the same

[1] E. Leung and R. D. Green, unpublished observations.

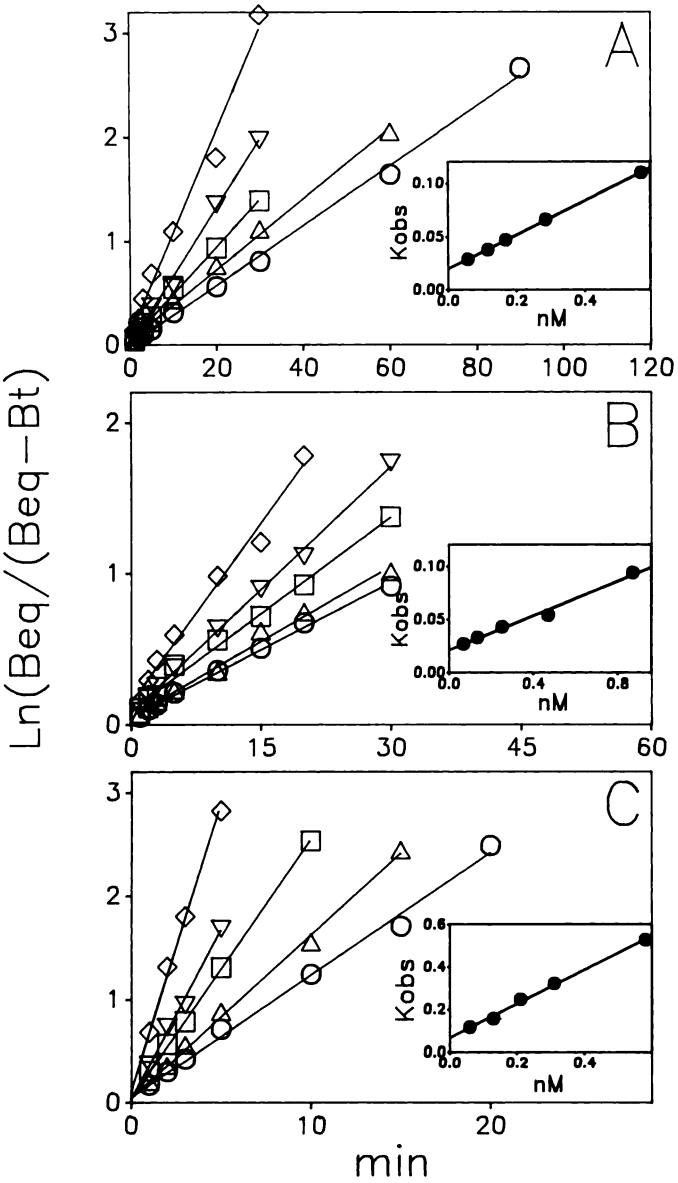

Fig. 1. Time course of (*R*)-[^{3}H]PIA (A), ^{125}I-ABA (B), and [^{3}H]CPX (C) binding to adenosine receptors in bovine cerebral cortical membranes. *Main panels*, semilogarithmic rate plots of specific [^{3}H]PIA binding at 0.06 (○), 0.12 (△), 0.17 (□), 0.29 (▽), and 0.56 nM (◇) (A), ^{125}I-ABA binding at 0.06 (○), 0.13 (△), 0.25 (□), 0.45 (▽), and 0.87 nM (◇) (B), and [^{3}H]CPX binding at 0.06 (○), 0.13 (△), 0.21 (□), 0.31 (▽), and 0.58 nM (◇) (C). *Insets*, plots of k_{obs} versus ligand concentrations. Values for k_{-1} (intercept of the secondary plot), k_{+1} (slope of the secondary plot), and K_{eq} (k_{-1}/k_{+1}) were 0.019 min^{-1}, 0.165 nM^{-1} min^{-1}, and 0.12 nM for (*R*)-[^{3}H]PIA; 0.021 min^{-1}, 0.122 nM^{-1} min^{-1}, and 0.17 nM for ^{125}I-ABA; and 0.067 min^{-1}, 0.802 nM^{-1} min^{-1}, and 0.084 nM for [^{3}H]CPX.

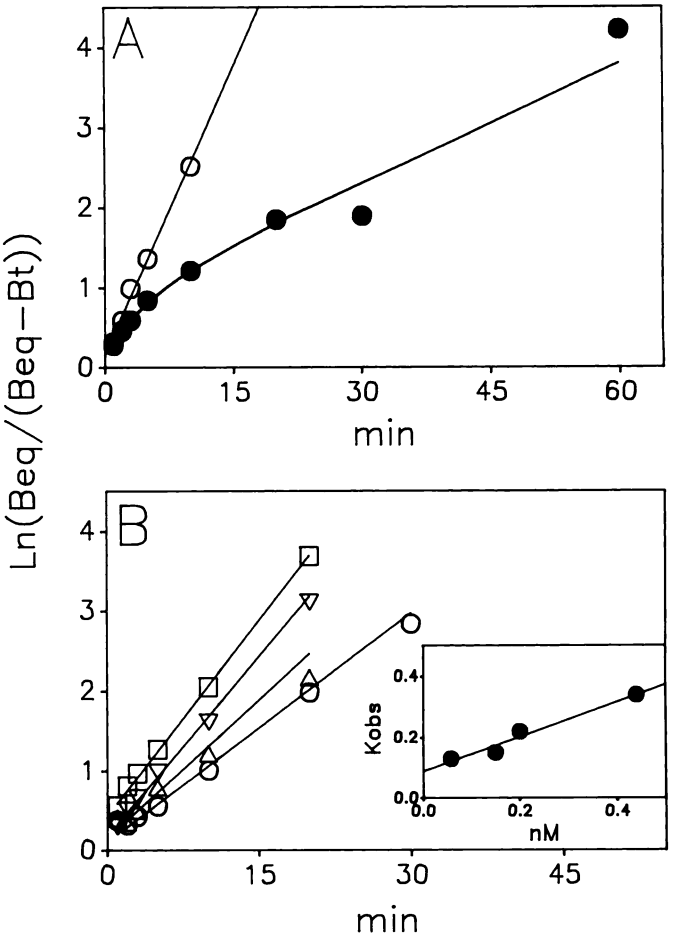

Fig. 2. Time course of [^{3}H]XAC binding to adenosine receptors in bovine cortical membranes. A, time course of specific [^{3}H]XAC binding (0.45 nM) in the absence (●) and in the presence of Gpp(NH)p (0.1 mM) (○). B, rate plots of [^{3}H]XAC binding [0.06 (○), 0.15 (△), 0.20 (▽), and 0.40 nM (□)] to receptors in NEM-pretreated membranes. *Inset*, secondary plot of these data (k_{+1} = 0.561 nM^{-1} min^{-1}, k_{-1} = 0.086 min^{-1}, and K_{eq} = 0.15 nM).

experiments, an example of which is summarized in Fig. 3. Scatchard plots are shown in the *main panels*; saturation isotherms are shown in the *insets*. Table 1A summarizes the K_d and B_{max} values from four such experiments performed within a short time span. Table 1B summarizes a similar set of data obtained in conjunction with the dual-isotope experiments discussed below. This latter group of experiments included ^{125}I-ABA. As would be expected, the B_{max} values of the agonist radioligands, (*R*)-[^{3}H]PIA and ^{125}I-ABA, were less than those of the antagonist radioligands, [^{3}H]XAC and [^{3}H]CPX. Unexpectedly, the B_{max} of [^{3}H]CPX appeared to be about 15–20% greater than that of [^{3}H]XAC. Although this small difference could be due to an error in the assigned specific activity of one or both of the radioligands, the same results were obtained with two lots of each radioligand with different assigned specific activities, and the B_{max} values for the binding of the two radioligands to digitonin-solubilized receptors were not statistically different. (In four paired experiments, B_{max} values were 507 ± 72 and 543 ± 86 fmol/mg for [^{3}H]XAC and [^{3}H]CPX, respectively.) It is also clear from the two groups of experiments summarized in Table 1 that this difference was reproducible.

Interactions between a constant low concentration of the antagonist radioligand [^{3}H]XAC and increasing concentrations of unlabeled agonists. Dissociation constants of competing ligands are often calculated from antagonist radioligand/unlabeled ligand inhibition curves using the Cheng and Prusoff correction if the pseudo-Hill coefficient (n_H) of the inhibition curve is 1 or by means of a computer program such as LIGAND if n_H is <1 (26). The latter analysis is based on a model of multiple noninteracting noninterconvertible sites. Fig. 4 shows a representative experiment in which the abilities of (*R*)-PIA and I-ABA to inhibit [^{3}H]XAC binding under various conditions were determined. Table 2 summarizes the analyses of three such experiments. These data were analyzed with

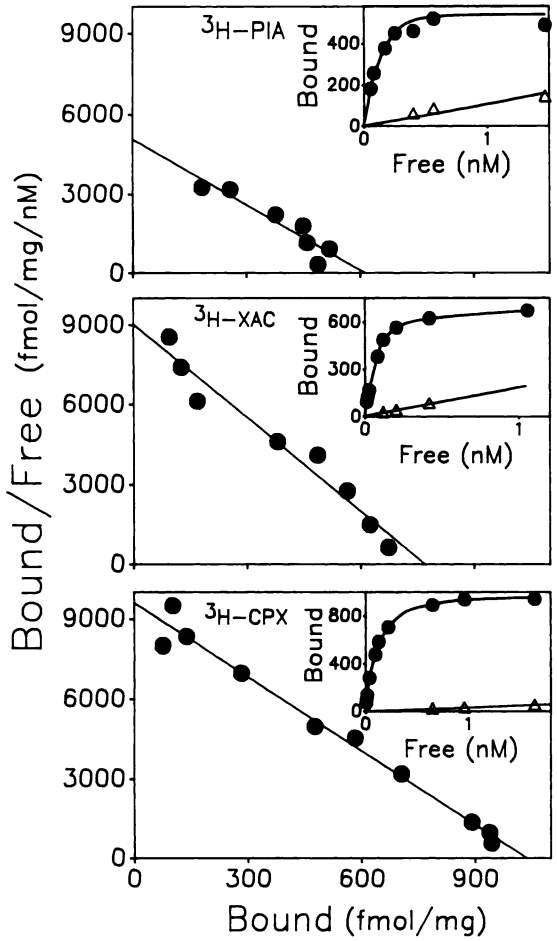

Fig. 3. Binding of [^{3}H]PIA (*top*), [^{3}H]XAC (*middle*), and [^{3}H]CPX (*bottom*) to adenosine receptors in bovine cortical membranes. The three different ligands were investigated in the same experiment. *Main panels*, Scatchard plots; *insets*, saturation isotherms of specific (●) and nonspecific binding (△). K_d and B_{max} values from four such experiments are summarized in Table 1.

TABLE 1

K_d and B_{max} values for ligand binding to adenosine receptors in bovine brain membranes

	Ligand	K_d	B_{max}	
		nM	fmol/mg	% of CPX value
A.	[^{3}H]CPX	0.14 ± 0.02	726 ± 127	100
	[^{3}H]XAC	0.12 ± 0.02	568 ± 88	79 ± 3
	(*R*)-[^{3}H]PIA	0.15 ± 0.03	428 ± 75	59 ± 3
B.	[^{3}H]CPX	0.17 ± 0.01	700 ± 36	
	[^{3}H]XAC	0.13 ± 0.02	560 ± 27	
	(*R*)-[^{3}H]PIA	0.17 ± 0.04	476 ± 47	
	^{125}I-ABA	0.12 ± 0.01	460 ± 36	

LIGAND; both K_H and K_L values are given when the analysis with LIGAND suggested that a two-site fit was significantly better than a one-site fit. Under control conditions, both agonists fit the two-site model. Even though Gpp(NH)p shifted the inhibition curve of (*R*)-PIA, according to this analysis (*R*)-PIA bound to two "sites" in the presence of Gpp(NH)p (similar results were obtained in a single experiment with I-ABA; data not shown). Both (*R*)-PIA and I-ABA bound to one site in NEM-pretreated membranes.

Interactions between variable concentrations of radioligands and constant concentrations of competing unlabeled ligands. Fig. 5 shows a representative experiment in

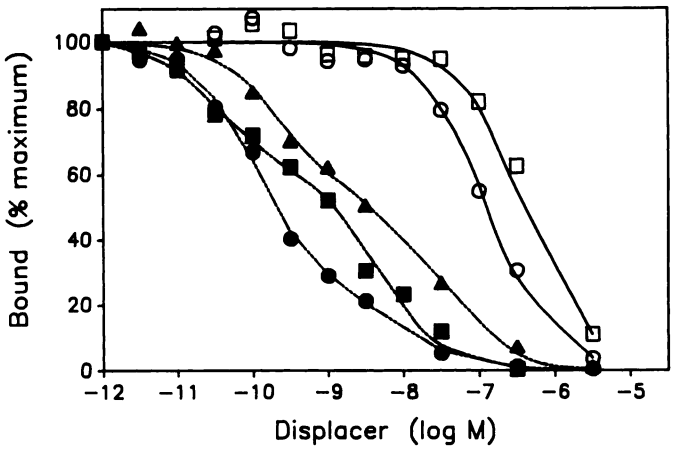

Fig. 4. [^{3}H]XAC-agonist inhibition curves. The concentration of [^{3}H]XAC was 0.36 nM. For (*R*)-PIA, ●, control; ▲, 0.1 mM Gpp(NH)p; and ○, NEM-pretreated membranes. For I-ABA, ■, control; and □, NEM-pretreated membranes.

which Scatchard plots of the antagonist radioligand [^{3}H]CPX with or without 20 nM (*R*)-PIA and the agonist radioligand (*R*)-[^{3}H]PIA with or without 2 nM CPX were determined. (The data summarized in Table 1A are actually from part of this set of experiments.) The parameters derived from these experiments and similar experiments with XAC and [^{3}H]XAC are summarized in Table 3. (*R*)-PIA (20 nM) increased the apparent K_d values of the antagonist radioligands 2–3-fold and severely reduced their B_{max} values. Table 3A also gives predicted K_d and B_{max} values of the radioligands in the presence of (*R*)-PIA, based on the independent two-site model in which the antagonist binds to the two sites with equal affinity and a K_d equal to that determined directly and (*R*)-PIA binds to the two sites with K_d values equal to the K_H and K_L values determined from the inhibition curves according to the independent site model. The theoretical curve based on this model for the experiment summarized in Fig. 5A is also shown in Fig. 5A, *inset*. According to the independent two-site model, the binding of the antagonist radioligand in the presence of the agonist would be to the site with low agonist affinity; the high affinity agonist site would not be detected in the experiment. Although the experimental fit deviated somewhat from that predicted, it is difficult to strongly argue that this deviation is sufficient to reject the two-independent site model.

If (*R*)-PIA binds to two independent sites with different affinities and only high affinity binding is detected directly by (*R*)-[^{3}H]PIA, then we would expect the presence of an antagonist to cause a predictable increase in the K_d of the agonist radioligand ($K_{d_{apparent}} = K_d$ (1 + [antagonist]/$K_{d_{antagonist}}$)); the B_{max} of the agonist should be unaffected. The experiment shown in Fig. 5B and the data summarized in Table 3B show that this does not occur. Neither CPX or XAC increased the $K_{d_{apparent}}$ of (*R*)-[^{3}H]PIA as expected; both antagonists reduced the number of sites detected by (*R*)-[^{3}H]PIA. These data are, therefore, incompatible with the independent two-site model.

Sucrose gradient centrifugation of solubilized adenosine receptors. We have previously found that the density gradient profiles of adenosine receptors detected by [^{3}H]XAC are different when the receptors are labeled before solubilization as compared with after sucrose gradient centrifugation, whereas the location of the receptors detected by the agonist ^{125}I-ABA is the same under the two conditions (18). Because

TABLE 2

Analysis of the inhibition of [^{3}H]XAC binding by I-ABA and (*R*)-PIA

K_H and K_L are the dissociation constants determined by analysis with *LIGAND*.

	IC_{50}	n_H	K_H	K_L	High affinity binding
	nM		nM		%
(*R*)-PIA					
Control	3.2 ± 1.5	0.52 ± 0.05	0.03 ± 0.02	10 ± 4.9	76
Gpp(NH)p	10.0 ± 5.2	0.48 ± 0.03	0.19 ± 0.12	32 ± 8.0	53
NEM	250 ± 130	0.91 ± 0.08	ND[a]	64 ± 4	
I-ABA					
Control	1.7 ± 0.52	0.50 ± 0.09	0.21 ± 0.11	18 ± 12.9	78
NEM	940 ± 300	1.0 ± 0.02	ND	296 ± 20	

[a] ND, not detectable.

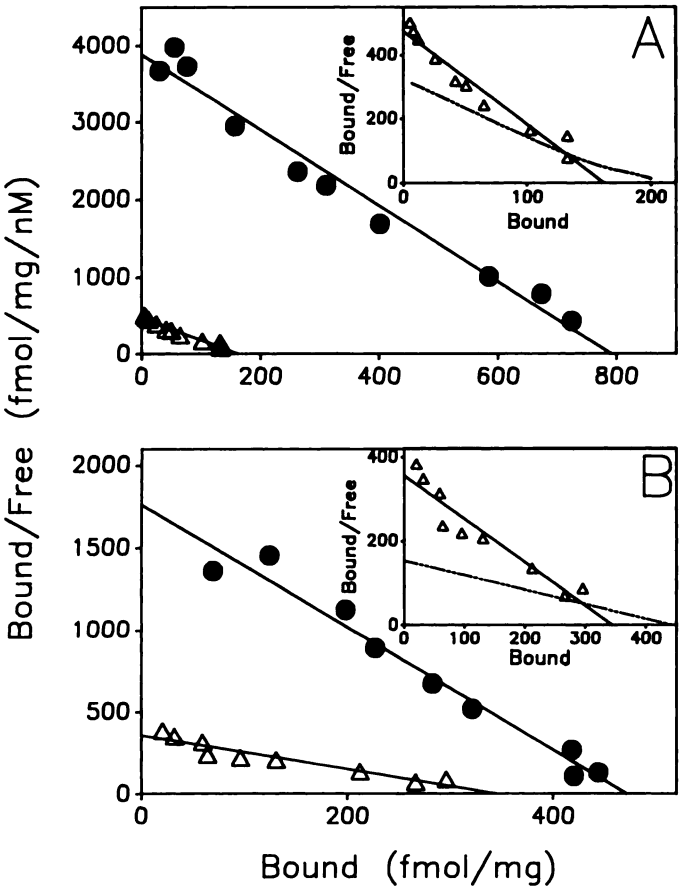

Fig. 5. Binding of [^{3}H]XAC in the absence and presence of PIA (20 nM) (A) and the binding of [^{3}H]PIA in the absence and presence of XAC (2 nM) (B). *Main panels*, Scatchard plots in the absence (●) and presence of competitor (△). *Insets*, Scatchard plots in the presence of competitors on enlarged scales. *Dashed lines in the insets*, theoretical fits based on the independent two-site model. These studies were part of the same experiment as presented in Fig. 3.

the receptors labeled by [^{3}H]XAC before solubilization were in lighter density fractions, as compared with those labeled by ^{125}I-ABA or those detected by [^{3}H]XAC after sucrose gradient centrifugation, we postulated that most of the adenosine receptors in the membrane are precoupled to a G protein and that [^{3}H]XAC binds with higher affinity to free receptors and destabilizes precoupled receptor-G protein complexes (18). Such an antagonist-induced dissociation of receptor-G protein complexes would be dependent on the antagonist having a more

TABLE 3

Interactions between agonist and antagonists as measured by Scatchard analyses of radioligand binding with and without unlabeled competing ligands

Control data are the same as those given in Table 1A. Site 1 is the low affinity site for agonist based on the independent two-site model. Site 2 is the high affinity site for agonist based on the independent two-site model.

	[^{3}H]XAC		[^{3}H]CPX	
	K_d	B_{max}	K_d	B_{max}
	nM	fmol/mg of protein	nM	fmol/mg of protein
A. Effect of (*R*)-PIA (20 nM) on the binding of [^{3}H]XAC and [^{3}H]CPX				
Control	0.12 ± 0.02	568 ± 88	0.14 ± 0.02	726 ± 12
(*R*)-PIA, 20 nM				
Experimental	0.36 ± 0.14	109 ± 23	0.29 ± 0.03	125 ± 25
Theoretical				
Site 1	0.36	136	0.42	136
Site 2	80.1	432	93.5	432
Unlabeled ligand		K_d	B_{max}	
		nM	fmol/mg of protein	
B. Effect of CPX (2 nM) and XAC (2 nM) on (*R*)-[^{3}H]PIA				
Control (none)		0.15 ± 0.03	428 ± 75	
XAC				
Experimental		1.00 ± 0.36	178 ± 55	
Theoretical		2.6	428	
CPX				
Experimental		0.81 ± 0.14	287 ± 63	
Theoretical		2.3	428	

favorable K_d for the free receptor than for the receptor-G protein complex (and consequently G proteins have a less favorable K_d for binding to antagonist-occupied receptors than for binding to free receptors) and could vary for different antagonists. Fig. 6 shows the sucrose gradient profiles obtained when the receptors were labeled with ^{125}I-ABA or [^{3}H]CPX before solubilization or with [^{3}H]CPX after solubilization and sucrose gradient centrifugation. Like previously reported for the antagonist [^{3}H]XAC, the receptors labeled by [^{3}H]CPX before solubilization were in lighter fractions compared with those labeled by ^{125}I-ABA before solubilization or those labeled by [^{3}H]CPX after solubilization and sucrose gradient centrifugation. Thus, [^{3}H]CPX, like [^{3}H]XAC, appears to preferentially bind to free receptors and to destabilize receptor-G protein complexes.

Interactions between agonist and antagonist radioligands. The availability of the ^{125}I-agonist radioligand ^{125}I-ABA and the two [^{3}H]antagonist radioligands [^{3}H]XAC and [^{3}H]CPX allows for the measurement of agonist-agonist and agonist-antagonist interactions in the same samples (see Experi-

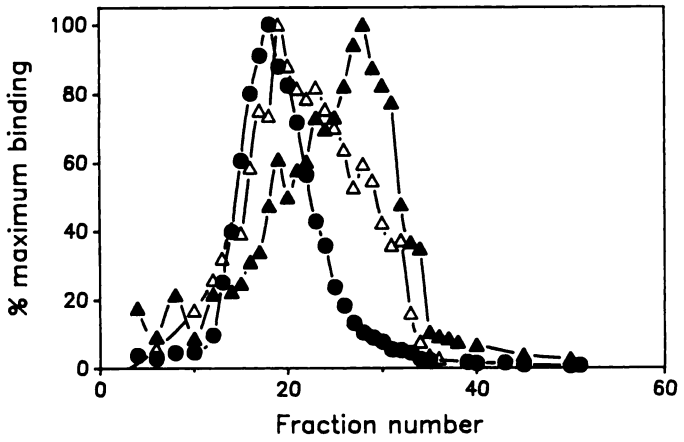

Fig. 6. Sucrose density gradient profiles of membrane-labeled adenosine A_1 receptors using the agonist radioligand ^{125}I-ABA (●) and the antagonist radioligand [^{3}H]CPX (▲) and receptors labeled by [^{3}H]CPX after sucrose gradient centrifugation (postgradient labeling) (△). Samples for postgradient labeling were incubated with [^{3}H]CPX (1 nM) for 20 min at 37° and harvested by filtration through polyethylenimine-soaked GF/B filters. The *left side* of the figure is the bottom of the gradient. The radioactivities attributable to specific binding in the peak fractions for ^{125}I-ABA, [^{3}H]CPX (membrane labeled), and [^{3}H]CPX (postgradient labeled) were 34,393, 1,478, and 3,951 dpm, respectively.

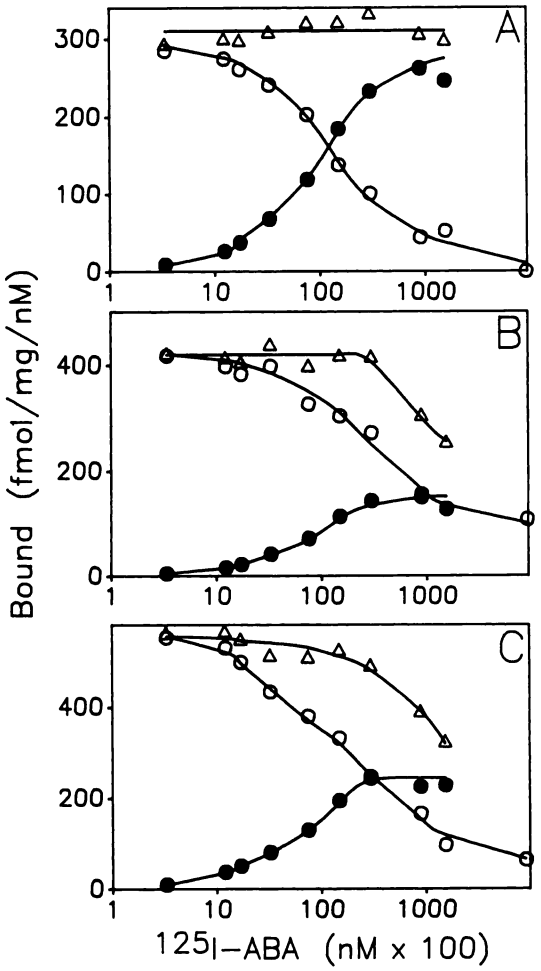

Fig. 7. Saturation isotherms of ^{125}I-ABA in the presence of 2 nM [^{3}H]PIA (A), 2.1 nM [^{3}H]XAC (B), or 1.9 nM [^{3}H]CPX (C). Specifically bound ^{125}I-ABA (●), ^{3}H-labeled competitor (○), and total ligand bound (△) are plotted against the concentrations of ^{125}I-ABA (logarithmic scale). The *lines* shown were drawn visually.

mental Procedures). Fig. 7 summarizes an experiment in which the interactions between high (much greater than the apparent K_d) concentrations of (*R*)-[^{3}H]PIA, [^{3}H]XAC, or [^{3}H]CPX and increasing concentrations of ^{125}I-ABA were determined. All amounts bound are in terms of fmol/mg and are corrected for nonspecific binding. Fig. 7A shows the interaction between the high concentration of (*R*)-[^{3}H]PIA (2 nM) and increasing concentrations of ^{125}I-ABA. It is evident that, as the concentration of ^{125}I-ABA increased, the amount of ^{125}I-ABA bound increased and the amount of (*R*)-[^{3}H]PIA bound stoichiometrically decreased, so that total ligand bound remained constant. This experiment also included a series of samples containing ^{125}I-ABA in the absence of (*R*)-[^{3}H]PIA so that Scatchard plots of ^{125}I-ABA with and without (*R*)-PIA could be constructed. The B_{max} in the presence of (*R*)-PIA was unaffected (92% of control) and the apparent K_d was 1.20 nM, which is in good agreement with the predicted shift (K_d of control, $[1 + I/K_i]$ = 1.19 nM). These results are indicative of a competitive interaction between the two agonist radioligands.

Fig. 7B shows the interaction between the high concentration of [^{3}H]XAC (2.1 nM) and increasing concentrations of ^{125}I-ABA. This interaction is clearly different from the interaction observed between (*R*)-[^{3}H]PIA and ^{125}I-ABA. Notably, 1) the reduction in antagonist binding with increasing concentrations of the agonist was much greater than the binding of the agonist and, consequently, the total ligand bound actually decreased at higher concentrations of ^{125}I-ABA and 2) there was a residual amount of specific [^{3}H]XAC binding (assessed using theophylline to define nonspecific binding) that was resistant to displacement by the concentrations of ^{125}I-ABA studied. A control ^{125}I-ABA Scatchard plot showed that the B_{max} of ^{125}I-ABA was decreased by 38% in the presence of [^{3}H]XAC. The interaction between the antagonist [^{3}H]CPX (1.9 nM) and the agonist ^{125}I-ABA was also determined in the same experiment; the results of this part of the experiment are summarized in Fig. 7C. Again, the interaction between the antagonist and agonist appeared to be nonstoichiometric. The B_{max} of ^{125}I-ABA was decreased by 17% in the presence of [^{3}H]CPX. The total number of sites labeled also decreased as the concentration of ^{125}I-ABA was increased.

Separation of bound and free ligand by centrifugation. One possible explanation for the lack of stoichiometry between the binding of ^{125}I-ABA and the displacement of bound [^{3}H]CPX or [^{3}H]XAC as the concentration of ^{125}I-ABA increased (Fig. 7) could be that ^{125}I-ABA forms a complex with the receptor that is not detected by the filtration assay. Because modeling (discussion deferred to Discussion) suggested the possible presence of a second relatively high affinity ^{125}I-ABA-receptor complex, we performed a series of experiments in which we measured ligand binding by both filtration and centrifugation. Fig. 8 shows saturation isotherms and Scatchard analyses of ^{125}I-ABA binding, as determined by filtration and by centrifugation. Data from similar experiments with ^{125}I-ABA, (*R*)-[^{3}H]PIA, and [^{3}H]CPX are summarized in Table 4. Even though the Scatchard plots of ^{125}I-ABA binding determined by centrifugation appeared to be curved, the number of data points was limited and the two-site fit was not significantly better than the one-site fit; nevertheless, parameter estimates for both one-site and two-site fits are given. More sites for the two agonists were detected by centrifugation as compared with filtration (Table 4). Although the Scatchard plots of (*R*)-[^{3}H]

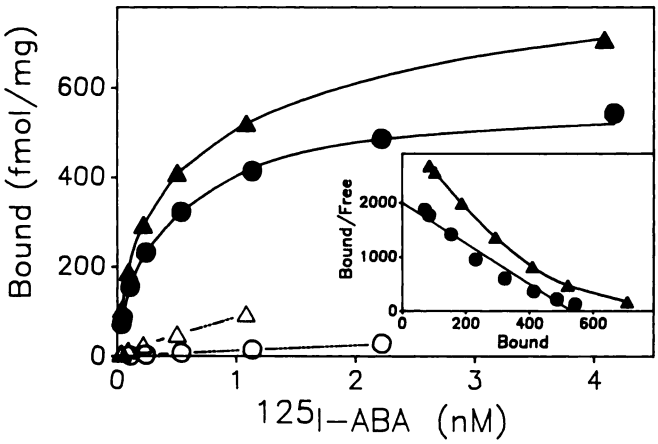

Fig. 8. Saturation analyses of ^{125}I-ABA binding to adenosine receptors in bovine cortical membranes using filtration and centrifugation to separate bound and free radioligand. *Main panel*, saturation isotherms of specific binding (*closed symbols*) and nonspecific binding (*open symbols*) determined by centrifugation (*triangles*) and filtration (*circles*). *Inset*, Scatchard plots of specific ^{125}I-ABA binding determined by the two different techniques.

TABLE 4

Comparison of radioligand binding parameters determined using filtration versus centrifugation to measure bound ligand

Parameters shown are mean K_d values ± standard errors determined by least square analyses of linear Scatchard plots or by EQUIL for the curvilinear Scatchard plots for ^{125}I-ABA obtained when bound ligand was separated by centrifugation. B_{max} values are shown in parentheses. There were three determinations for each set of experiments.

Ligand	K_d	
	Filtration	Centrifugation
^{125}I-ABA		
1-site fit	0.27 ± 0.01 (455 ± 83)	0.31 ± 0.02 (628 ± 104)
2-site fit	ND[a]	K_H 0.13 ± 0.10 (320 ± 57) K_L 2.2 ± 3.3 (440 ± 56)
(*R*)-[^{3}H]PIA	0.45 ± 0.04 (498 ± 8)	0.74 ± 0.23 (610 ± 33)
[^{3}H]CPX	0.23 ± 0.05 (970 ± 50)	0.32 ± 0.04 (940 ± 28)

[a] ND, not determined.

PIA binding were not noticibly curvilinear (plots not shown), the extra binding of the two agonists detected by centrifugation was most likely due to a second species of agonist-receptor complexes, because the rate of dissociation of the agonists from the site detected by filtration was slow ($t_{1/2} \geq 30$ min), suggesting that all of this site was detected by filtration. The numbers of sites detected by [^{3}H]CPX using filtration and centrifugation were the same (Table 4).

Discussion

Complex binding data (curvilinear Scatchard plots and antagonist radioligand-unlabeled agonist competition curves with pseudo-Hill coefficients of ≤ 1) are commonly analyzed with computer programs such as LIGAND, which are based on a noninteracting independent site model. In 1980 DeLean *et al.* (29) published their work in which they analyzed β-adrenergic receptor ligand binding data with this and other models. Although a two-independent site model adequately fit their data, they rejected this model as a viable mechanistic model to describe ligand binding to a receptor that couples to a G protein. They proposed a ternary complex model, a model formally identical to the mobile receptor model developed independently by Jacobs and Cuatracasas (30), to describe the system. For the β-adrenergic receptor, this hypothesis states that 1) in the absence of an agonist, most of the receptor exists uncoupled from G_s, 2) agonist binding to the receptor stabilizes a ternary complex consisting of the agonist, the receptor, and G_s liganded with GDP, and 3) antagonists bind to uncoupled and coupled receptors with equal affinities. The binding of the receptor to G_s facilitates the exchange of GTP for the bound GDP, which activates the G protein and destabilizes the ternary complex, thus releasing free receptor. Limbird and Lefkowitz (21) performed gel exclusion chromatographic studies that provided physical evidence for this model. Briefly, they showed that 1) antagonist but not agonist radioligands form high affinity complexes with detergent-solubilized β-adrenergic receptors, 2) the apparent molecular weight of β-adrenergic receptors solubilized in the presence of an agonist radioligand is greater than that of receptors solubilized in the presence of an antagonist radioligand, and 3) the apparent molecular weight of β-adrenergic receptors labeled with an antagonist radioligand is the same when the receptors are labeled before or after solubilization. Although this model or variations of this model are widely accepted for receptor systems that are coupled to effectors via G proteins, as mentioned above, antagonist radioligand-agonist competition curves are widely analyzed based on the independent site model. Abramson *et al.* (31) generated data with a ternary complex model [nonselective antagonist, selective agonist, receptor concentration > G protein concentration ($[R] > [G]$)], which they subsequently analyzed with an independent site model. They showed that under these conditions the two-independent site model gives good estimates of 1) the affinity of the agonist for the (free) receptor (K_L) and 2) the concentration of the regulatory component ($[G]$). Reliable estimates of the other affinity constants relating to the ternary complex model are not obtained.

The A_1-adenosine receptor behaves differently from the β-adrenergic receptor in that agonist radioligands bind to detergent-solubilized receptors with high affinity (16, 18, 19). We recently reported experiments using sucrose gradient centrifugation that further contrasted the behavior of adenosine and β-adrenergic receptors (18). These studies showed that the apparent size of the adenosine receptors labeled with the agonist ^{125}I-ABA before solubilization or after solubilization and sucrose gradient centrifugation is the same, whereas the apparent size of the receptor labeled by the antagonist [^{3}H]XAC before solubilization is less than that detected by the antagonist after solubilization and sucrose gradient centrifugation. The results of the experiment summarized in Fig. 6 show that these results are not peculiar to [^{3}H]XAC, in that identical results are obtained with [^{3}H]CPX. We previously suggested that 1) adenosine receptors are strongly coupled to a G protein in the absence of an agonist and that this complex is stable to detergent solubilization, 2) antagonists preferentially bind to free receptors, i.e., antagonists have a more favorable K_d for the free receptor than for the receptor-G protein complex, and 3) antagonists destabilize precoupled receptor-G protein complexes. If these hypotheses are correct, then interactions between adenosine receptor agonists and antagonists, although competitive in the sense that both types of ligands bind to the same site, will appear noncompetitive in nature.

Saturation analyses of agonist radioligand binding in the absence and presence of unlabeled antagonist and antagonist radioligand binding in the absence and presence of unlabeled

agonist (Fig. 5; Table 3) were performed to further probe the mechanisms underlying the agonist-antagonist interactions. Although the agonist (*R*)-PIA decreased the B_{max} of the antagonists, as predicted by a ternary complex model in which antagonists destabilize precoupled *RG* complexes (32), similar results can occur with an independent two-site model (Fig. 5A) or a ternary complex model (fit not shown) in which the antagonist is nonselective and the agonist is selective.

The effects of the antagonists on the agonist Scatchard plots were more helpful in differentiating between prospective models. Because the agonist radioligand only detects the high affinity state, the antagonism of this binding by antagonists should have the characteristics of competitive antagonism. Fig. 5B shows an experiment of this type, along with the curve predicted by the independent site model. The experimental results were at variance with the independent site model. Further simulations based on a ternary complex model in which the agonist affinity for *RG* is greater than for *R* and the antagonist has equal affinities for the two forms of the receptor were performed (not shown). This model also did not appear to adequately account for the results. The results are compatible with models in which both agonists and antagonists are selective for different forms of the receptor [see Wreggett and De Lean (32)]. Analyses of actual data with models based on antagonist selectivity or nonselectivity are given below. It should be noted that qualitatively similar results for the interaction of another alkylxanthine and [^{3}H]CHA at rat brain A_1-adenosine receptors have been reported by Williams *et al.* (33).

The availability of both ^{3}H- and ^{125}I-labeled radioligands allowed us to further probe the interactions between agonists and antagonists using dual-isotope methodology (Fig. 7). As a positive control, we looked at the interactions between two agonists, ^{125}I-ABA and (*R*)-[^{3}H]PIA; these two ligands interacted competitively, as one would predict (Fig. 7A). The apparently greater than stoichiometric displacement of ^{3}H-antagonists by the agonist ^{125}I-ABA (Fig. 7, B and C) was evident immediately. This suggested the possible presence of a rapidly dissociating species of ^{125}I-ABA-receptor complex. Experiments in which bound radioligand was estimated using centrifugation rather than filtration (Fig. 8) confirmed the presence of such a species.

We have utilized the computer program EQUIL to attempt to establish models consistent with all of our experimental data. A plausible model had to be consistent with many different observations from different types of experiments. It was clear from the radioligand antagonist-agonist competition curves (Fig. 4) that the K_L for the agonists was not the same as the K_d determined in NEM-treated membranes. It was also clear that Gpp(NH)p decreased the affinity of the receptor for agonists but that more than one state or site remained in the presence of a high concentration of guanine nucleotide. These results were incompatible with an independent site model and, furthermore, indicated that more than two states of the receptor must exist. The existence of more than one agonist high affinity state was suggested in the dual-isotope experiments (Fig. 7) and confirmed when ligand binding was measured by both filtration and centrifugation (Fig. 8). Lastly, sucrose density gradient experiments (Fig. 6) suggested that adenosine receptors couple to a G protein in the absence of an agonist, i.e., are precoupled, and that adenosine receptor antagonists cause the dissociation of precoupled receptor-G protein complexes.

Therefore, as a starting point for our modeling, we assumed that 1) the total receptor concentration is estimated by the antagonist B_{max}, 2) the dissociation constant describing the binding of the receptor to the G protein is such that the formation of receptor-G protein complexes is favored at the concentrations of reactants present, 3) agonists preferentially bind to receptor-G protein complexes, whereas antagonists preferentially bind to free receptors, and 4) agonists bind to two distinct forms of the receptor with high affinity. In all analyses we constrained the K_d for ^{125}I-ABA binding to free receptor at 300 nM. This was the K_d for I-ABA inhibition of [^{3}H]XAC binding in NEM-pretreated membranes (Table 2). Although the possibility that NEM treatment affects agonist binding to free receptors cannot be absolutely ruled out, the use of this K_d would seem reasonable, because the K_d of I-ABA determined by the inhibition of [^{3}H]XAC binding to solubilized receptors in the presence of Gpp(NH)p was the same (data not shown) and Nakata (34) reported that NEM treatment does not affect the binding of [^{3}H]CPX to A_1 receptors purified from rat testis. Our approach was to simultaneously fit all the data in the dual-isotope experiments utilizing [^{3}H]CPX and ^{125}I-ABA. (A representative experiment without the control agonist and antagonist Scatchard plots is shown in Fig. 7C.) A simple ternary complex model involving one receptor and one G protein was obviously inadequate because this model only has two receptor states, *R* and *RG*. We, therefore, investigated a model with one receptor type and two G proteins (Fig. 9, model 1) and a model with two receptor types and one G protein (Fig. 9, model 2). Both models give physical explanations for two high affinity sites for the agonist and one high affinity site for the antagonist. The data were well fit by both of these models.

For model 1, the two G proteins, symbolically represented as G_1 and G_2, could be two different G proteins such as G_i and G_o or could be two distinct states of one G protein, such as G_i with GDP bound and G_i without a guanine nucleotide bound. We assumed that, experimentally, we measure binding of the antagonist to the free receptor and started the analysis with the experimentally determined K_d of [^{3}H]CPX. Similarly, we assumed that the K_d of ^{125}I-ABA measured by filtration is an estimate of K_d for the binding of the agonist to RG_1. An initial value for the K_d for the agonist binding to RG_2 was obtained from simulations of the "phantom" site in the dual-isotope experiments, i.e., by calculating the binding of ^{125}I-ABA to a second site assuming that the lack of stoichiometry between ^{125}I-ABA binding and [^{3}H]CPX displacement was due to a rapidly dissociating ^{125}I-ABA-receptor complex. The K_d for the binding of [^{3}H]CPX to the two coupled forms of the receptor was set to be very unfavorable and the same. This K_d was subsequently made more favorable; the parameters defining the affinities of the agonist for the two coupled forms of the receptor and the affinity of the antagonist for the uncoupled form of the receptor were unaffected as long as this K_d was $\leq$2 nM. The parameters shown in the model diagram (Fig. 9) are from the fit of the single experiment shown in Fig. 10. The values summarized in Table 5 are those determined by the simultaneous analysis of four such similar experiments. The same reasoning was used to fit the data to model 2. In this case the affinity constants for antagonist binding to the two types of uncoupled receptors were constrained to be the same, and affinity constants for the binding of the agonist to the two types of uncoupled receptors were set at 300 nM. Again, the

Model 1: 1 receptor, 2 G-proteins

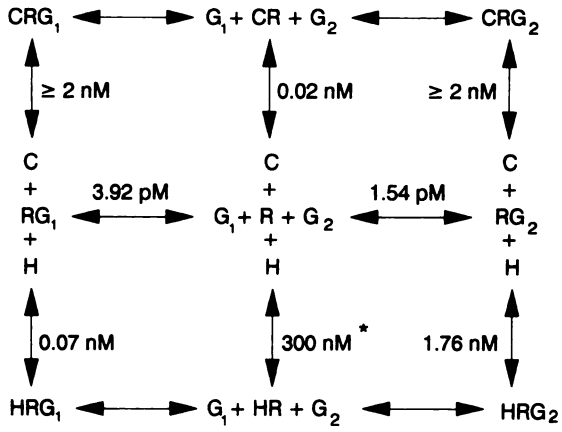

Model 2: 2 receptors, 1 G-protein

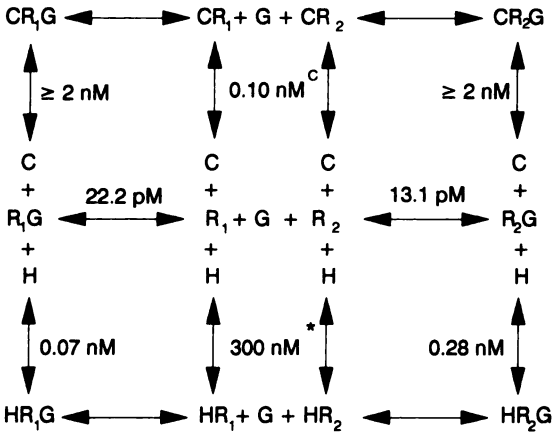

Fig. 9. Schematic representation of the two ternary complex models consistent with the interactions between the agonist ^{125}I-ABA (*H*) and the antagonist [^{3}H]CPX (*C*) at the adenosine A_1 receptor in the bovine cerebral cortex. In model 1, *R* is the adenosine A_1 receptor and G_1 and G_2 are the two G proteins that can couple to the receptor. In model 2, R_1 and R_2 are the two subtypes of A_1 receptor and *G* is the G protein that couples to the two types of receptor. The *asterisk* above the dissociation constant defining the affinity of the agonist for the free receptor(s) denotes that this value was treated as a constant. In model 2, the antagonist is also constrained to bind R_1 and R_2 with equal affinity. The dissociation constant(s) defining the affinity of the antagonist for the coupled receptor(s) is shown as ≥2 nM. This value was also treated as a constant during the computer fitting and did not affect the values of the other constants as long as it was held at ≥2 nM. Initial estimates of the other dissociation constants were assigned as discussed in the text and EQUIL was allowed to fit the experimental data to give the best estimates of the dissociation constants and the concentration of the reactants. The dissociation constants shown in this figure are those determined from the analysis of the single experiment shown in Fig. 10. Table 5 gives the parameter estimates obtained by the simultaneous fit of four such experiments.

values in the model diagram (Fig. 9) are for the fit of the single experiment shown in Fig. 10; Table 5 summarizes the parameters determined by the simultaneous fit of the four experiments.

The abilities of the two models to fit the experimental data did not differ significantly ($F = 1.34$, $p > 0.05$). Importantly, both models predicted that a high percentage of the receptors exist precoupled to a G protein(s) in the absence of an effector. The estimates of K_d values for the highest affinity site for agonist and for the high affinity antagonist site are similar for

TABLE 5

Summary of computer-fitted parameters for the binding of [^{3}H]CPX and ^{125}I-ABA according to model 1 (one receptor, two G proteins) and model 2 (two receptors, one G protein)

Values given for radioligands are dissociation constants in nM. Values given for reactants are concentrations in fmol/mg of protein. The values were generated by the simultaneous fit of four dual-isotope experiments. Standard errors are calculated from the product of the mean square of the fit and the diagonal components of the inverse second derivative of the weighted sum of squares. The model of variance used for weighing each measured concentration was $1 \times 10^{-30} + 0.0016 \times \text{concentration}^2$ (4% experimental error was assumed).

	High agonist affinity sites		Low agonist affinity site
Model 1	RG_1	RG_2	R
I-ABA	0.08 ± 0.002	0.44 ± 0.01	300[a]
CPX	≥2[a]	≥2[a]	0.02 ± 0.01
R = 872 ± 157, G_1 = 559 ± 82, G_2 = 814 ± 124, 85% R precoupled			
Model 2	R_1G	R_2G	R[a]
I-ABA	0.06 ± 0.01	0.19 ± 0.04	300[a]
CPX	≥2[a]	≥2[a]	0.05 ± 0.001
R_1 = 546 ± 149, R_2 = 538 ± 63, G = 1029 ± 172, 47% R_1 precoupled, 90% R_2 precoupled			

[a] Values constrained; for model 2, I-ABA and CPX are constrained to bind R_1 and R_2 with equal affinity.

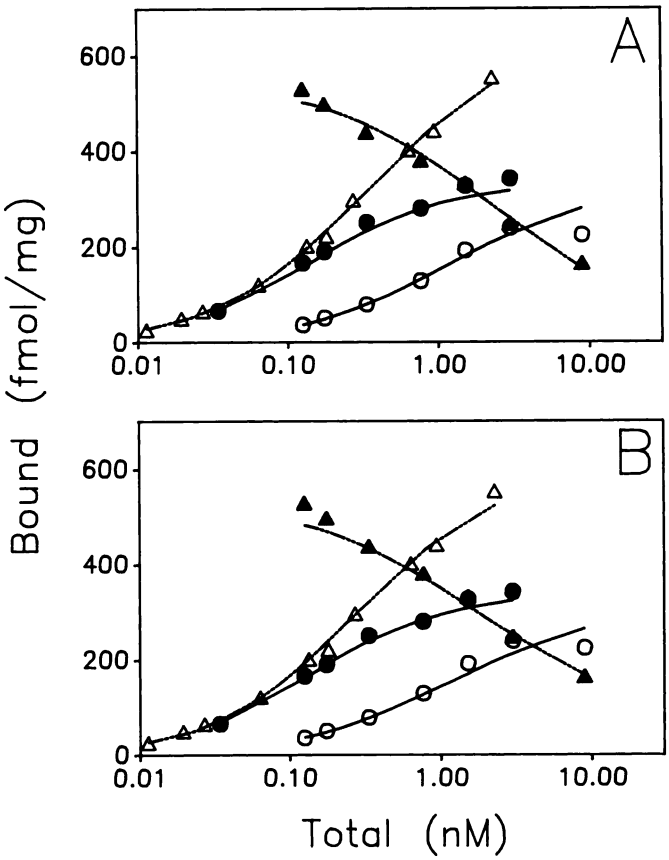

Fig. 10. Plots of all data points of an experiment in which saturation isotherms of ^{125}I-ABA alone (●) and in the presence of 1.9 nM [^{3}H]CPX (○) and a saturation isotherm for [^{3}H]CPX alone (△) were performed. The binding of [^{3}H]CPX (1.9 nM) as the concentration of ^{125}I-ABA increased is also shown (▲). Parts of this experiment were presented in Figs. 3 and 7. The *fitted lines* are those determined by the simultaneous analysis of all the data points by EQUIL using model 1 (A) and model 2 (B). The dissociation constants for these fits are given in Fig. 9.

the two models and are similar to those determined in direct Scatchard analyses (Table 1). Thus, these comparisons do not favor one model over the other; these comparisons do suggest that the experimentally determined values are reasonable estimates of "real" affinity constants. The computer-generated estimates of the affinity of the antagonist [^{3}H]CPX for free *R* are at greater variance with the experimentally generated value (2–10-fold difference, depending on the comparison made) than are the corresponding values for the agonist ^{125}I-ABA (1.5–2-fold). This could be explained by the favorable K_d values defining the interaction between *R* and *G*, which would cause an underestimation of the true affinity of the antagonist for *R*. Although treatment with NEM to uncouple *R* and *G* tended to lower the K_d estimate for [^{3}H]CPX, as would be predicted by this hypothesis, these experiments were hampered by an apparent instability of the receptors under these conditions, as previously discussed (data not shown). It should also be noted that the present analyses do not provide estimates of the affinities of the antagonists for any of the coupled forms of the receptor(s); these values were fixed at 2 nM for the analyses shown. Differences in the ratios of the affinities for the free receptor(s) (directly measured) and coupled forms of the receptor could account for differences in B_{max} values of different antagonists, such as the apparent difference between [^{3}H]CPX and [^{3}H]XAC (Table 1).

Our consideration of the experimental observations that had to be taken into account in developing models to define the "workings" of the adenosine receptor system included observations from sucrose gradient centrifugation studies. We interpreted these studies to suggest that antagonists exhibit preference for uncoupled receptors, a concept at variance with the commonly accepted dogma. We, therefore, reanalyzed the [^{3}H]CPX/^{125}I-ABA experiments with modifications of models 1 and 2 in which we assumed that [^{3}H]CPX binds to all states of the receptor with equal high affinity. For both models, in three of four experiments the data were statistically better fit by the antagonist-selective model. The deviations in the fit were most obvious for the ^{125}I-ABA saturation isotherms with or without CPX; for clarity, only these parts of an experiment with the theoretical fits are shown in the *main panel* of Fig. 11; the remaining parts along with the theoretical fits are shown in Fig. 11, *insets*. In the experiment in Fig. 11, which is different from that shown in Fig. 10, the selective antagonist model gave statistically better fits for both models 1 and 2 ($p < 0.05$, *F* test). In the experiment shown in Fig. 10 the selective antagonist model gave a statistically better fit for model 2, whereas the difference just missed significance for model 1. It is, thus, clear that these experiments, independent of the sucrose gradient centrifugation experiments, suggest that antagonists have preferential selectivity for free uncoupled receptors. Wreggett and De Lean (32) proposed that a similar situation occurs with D_2-dopamine receptors, in that they proposed that spiperone preferentially binds to uncoupled D_2 receptors. Although independent site models are not mechanistically appropriate for receptors that couple to G proteins, we also analyzed the same experiments with a two-independent site model in which one site binds agonist with high affinity and antagonist with low affinity, whereas the other site binds agonist with low affinity and antagonist with high affinity (data not shown). Both of the selective models based on the ternary complex model gave

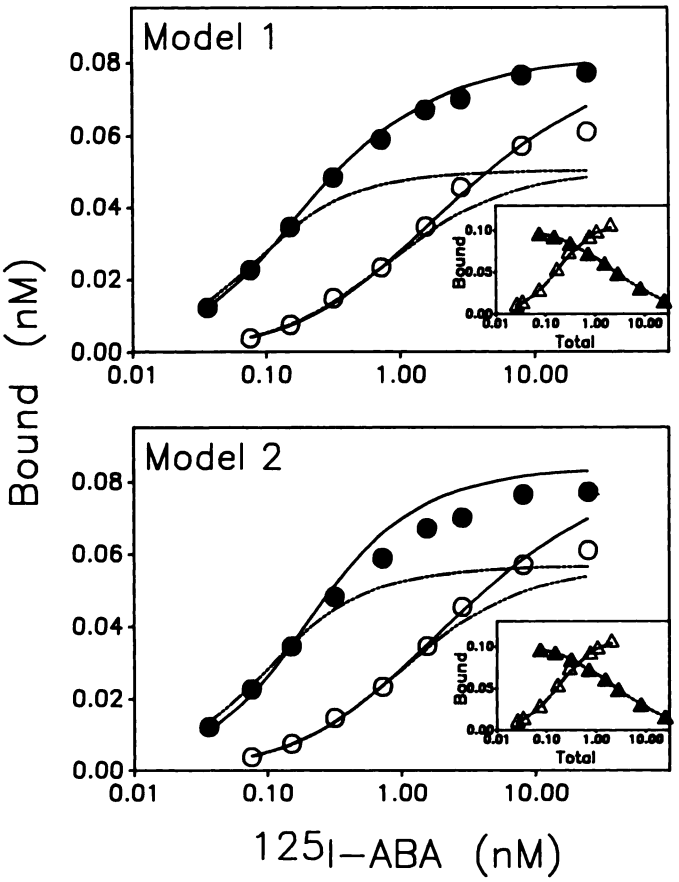

Fig. 11. Analysis of dual-isotope experiment ([^{3}H]CPX and ^{125}I-ABA) with modified versions of models 1 and 2 in which the affinity of [^{3}H]CPX for all forms of the receptor(s) was constrained to be equal. The data are from an experiment identical to the experiment shown in Fig. 10; the same symbols are used in both figures. For clarity, the *main panels* show the ^{125}I-ABA saturation isotherms with and without [^{3}H]CPX. The fits shown are for unmodified versions (selective antagonist affinities, *solid lines*) and modified versions (nonselective antagonist affinities, *broken lines*) of models 1 and 2. The remaining parts of the experiment, along with the fits for the modified versions of the models, are shown in the *insets*.

statistically better fits of the data, as compared with this model ($p < 0.001$).

The stability of A_1 receptor-G protein complexes in detergent solutions (19–20), along with the different characteristics of the association kinetics of [^{3}H]CPX (Fig. 1C) and [^{3}H]XAC (Fig. 2), at first might seem to conflict with the proposed models. This is not the case. Although the present experiments support the hypothesis that antagonists bind free receptors preferentially and destabilize precoupled receptor-G protein complexes, our earlier interpretation that the destabilization was due to the dissociation of receptor-G protein complexes to provide free receptor (18) may have been misleading. When an antagonist *C* is added to the system, it can bind to the free receptor *R* to form *CR* or to receptor-G protein complexes *RG* to form *CRG* (refer to appropriate portion of model 1 in Fig. 9). It is important to remember that the dissociation constants for the various reactions are ratios of their reverse and forward rate constants. It, therefore, follows that *C* may react quickly with *RG* to form *CRG*, even though the K_d for this reaction is less favorable than that for the formation of *CR*. It is easy to set rate constants so that the formation of *CR* is primarily due

to $C + RG \rightarrow CRG \rightarrow CR + G$ and the on-rate of ligand binding is either monophasic or more complex. The finding that the on-rate of the binding of [^{3}H]XAC was biphasic, whereas that of [^{3}H]CPX was monophasic, actually supports this route, because the binding of both radioligands would be biphasic if some receptors were initially uncoupled and the dissociation of *RG* to give free *R* was rate limiting. (This would imply, of course, that the k_{+1} determined experimentally for [^{3}H]CPX was not the forward rate constant for $C + R$ to form *CR*, as assumed, but rather that for *C* to bind to *RG* to form *CRG*.) Importantly, these considerations show how antagonists can destabilize *RG* complexes without causing a direct dissociation of *RG* to liberate free *R*.

Although the experimental data were fit equally well by the two models, the known ability of A_1 receptors to couple to multiple effectors (13, 14), along with recent reports showing that multiple receptor subtypes of other receptors exist [for example, muscarinic cholinergic receptors (35)] would tend to give credibility to model 2, i.e., the existence of subtypes of A_1 receptors with different pharmacological characteristics. On the other hand, the observation that G proteins (36) [specifically α_o, α_i, and α_{i3} (37)] copurify with A_1 receptors on an agonist affinity gel is in accord with model 1. In addition, Elazar *et al.* (38) recently reported that partially purified preparations of D_2-dopamine receptors prepared by antagonist affinity chromatography contain both α_i and α_o, both of which appear to be functionally coupled to the receptors. Thus, good cases for both models can be argued. An equally plausible possibility is that there is truth in both models, i.e., that there are multiple subtypes of receptors coupled to multiple types of G proteins. Due to its complexity, this possibility was not probed with the present approach.

Importantly, both of the proposed models predict that a sizable percentage of the receptors are coupled to a G protein(s) in the absence of an agonist and that the antagonists studied (XAC and CPX) have the potential to exert negative efficacies, i.e., to exert effects opposite to those of agonists (39). These models would predict that antagonists with equal affinities for the different forms of the receptor(s) would behave as competitive antagonists, whereas those with relatively greater affinities for free receptors could exhibit negative efficacies. The relative negative efficacies of different compounds would be related to differences in their relative specificities, with those compounds with greater specificity for free receptors exerting greater negative efficacies. It should be pointed out that all of the present experiments were performed in solutions of low ionic strength, which could affect the results. For example, Ehlert (40) has pointed out that the coupling of muscarinic receptors to G proteins may be increased in low ionic strength conditions. We have not performed experiments to determine the effects of addition of either Na^+ or K^+ to our solutions. Costa and Herz (41) reported that the expression of negative efficacies of δ-opioid receptor antagonists (measured as decreases in GTPase activity) is present in 150 mM NaCl but significantly amplified when NaCl is replaced by KCl. A recent report of Vannucci *et al.* (42) supports the hypotheses that A_1 receptor-G protein complexes may exert a tonic effect on an effector in the absence of an agonist and that A_1 antagonists may exert negative efficacies. These workers studied isolated fat cells in which A_1 receptors are coupled to the inhibition of adenylate cyclase. They reported that the cAMP content of fat cells (with high concentration of adenosine deaminase) from obese Zucker rats is less than that of lean Zucker rats and that 8-phenyltheophylline causes a dose-dependent elevation in the cAMP content of the fat cells from the obese Zucker rats. It would, thus, appear that A_1 adenosine receptors and other receptors may couple to G proteins in the absence of agonists under physiological conditions and that the pharmacological effects and mechanisms of action of other competitive antagonists should be carefully reconsidered.

Acknowledgments

We wish to acknowledge the technical assistance of Christine Bobichon in some of the experiments.

References

1. Williams, M., and K. A. Jacobson. Radioligand binding assays for adenosine receptors, in *Adenosine Receptors* (M. Williams, ed.). Human, Clifton, NJ, in press.
2. Jarvis, M. F. Autoradiographic localization and characterization of brain adenosine receptor subtypes, in *Receptor Localization: Ligand Autoradiography* (F. M. Leslie and C. A. Altar, eds.). Alan R. Liss, New York, 96–111 (1988).
3. Bruns, R. F., J. W. Daly, and S. H. Snyder. Adenosine receptors in brain membranes: binding of N^6-cyclohexyl[^{3}H]adenosine and 1,3-diethyl-8-[^{3}H]phenylxanthine. *Proc. Natl. Acad. Sci. USA* **77**:5547–5551 (1980).
4. Schwabe, U., and T. Trost. Characterization of adenosine receptors in rat brain by (−)[^{3}H]N^6-phenylisopropyladenosine. *Naunyn-Schmiedeberg's Arch. Pharmacol.* **313**:179–187 (1980).
5. Williams, M., and E. A. Risley. Biochemical characterization of putative central purinergic receptors by using 2-chloro[^{3}H]adenosine, stable analog of adenosine. *Proc. Natl. Acad. Sci. USA* **77**:6892–6896 (1980).
6. Williams, M., A. Braunwalder, and T. J. Erickson. Evaluation of the binding of the A-1 selective adenosine radioligand, cyclopentyladenosine (CPA), to rat brain tissue. *Naunyn-Schmiedeberg's Arch. Pharmacol.* **332**:179–183 (1986).
7. Linden, J. Purification and characterization of (−)[^{125}I]hydroxyphenylisopropyladenosine, an adenosine R-site radioligand. *Mol. Pharmacol.* **26**:414–423 (1984).
8. Linden, J., A. Patel, and S. Sadek. [^{125}I]Aminobenzyladenosine, a new radioligand with improved specific binding to adenosine receptors in heart. *Circ. Res.* **56**:279–284 (1985).
9. Jacobson, K. A., D. Ukena, K. L. Kirk, and J. W. Daly. [^{3}H]Xanthine amine congener of 1,3-dipropyl-8-phenylxanthine: an antagonist radioligand for adenosine receptors. *Proc. Natl. Acad. Sci. USA* **81**:4089–4093 (1986).
10. Lohse, M. J., K.-N. Klotz, J. Lindenborn-Fotinos, M. Reddington, U. Schwabe, and R. A. Olsson. 8-Cyclopentyl-1,3-dipropylxanthine (DPCPX): a selective high affinity antagonist radioligand for A_1 adenosine receptors. *Naunyn-Schmiedeberg's Arch. Pharmacol.* **336**:204–210 (1987).
11. Bruns, R. F., J. H. Fergus, E. W. Badger, J. A. Bristol, L. A. Santay, J. D. Hartman, S. J. Hays, and C. C. Huang. Binding of the A_1-selective adenosine antagonist 8-cyclopentyl-1,3-dipropylxanthine to rat brain membranes. *Naunyn-Schmiedeberg's Arch. Pharmacol.* **335**:59–63 (1987).
12. Patel, A., R. H. Craig, S. M. Daluge, and J. Linden. [^{125}I]BW-A844U, an antagonist radioligand with high affinity and selectivity for adenosine A_1 receptors, and [^{125}I]-azido-BW-A844U, a photoaffinity label. *Mol. Pharmacol.* **33**:585–591 (1988).
13. Yeung, S.-M. H., and R. D. Green. Agonist and antagonist affinities for inhibitory adenosine receptors are reciprocally affected by 5′-guanylylimidodiphosphate or *N*-ethylmaleimide. *J. Biol. Chem.* **258**:2334–2339 (1983).
14. Trussell, L. O., and M. B. Jackson. Dependence of an adenosine-activated potassium current on a GTP-binding protein in mammalian central neurons. *J. Neurosci.* **10**:3306–3316 (1987).
15. Ramkumar, V., and G. L. Stiles. Reciprocal modulation of agonist and antagonist binding to A_1 adenosine receptors by guanine nucleotides is mediated via a pertussis toxin-sensitive G protein. *J. Pharmacol. Exp. Ther.* **246**:1184–1200 (1988).
16. Stiles, G. L. A_1 adenosine receptor-G-protein coupling in bovine brain membranes: effects of guanine nucleotides, salt, and solubilization. *J. Neurochem.* **51**:1592–1598 (1988).
17. Lohse, M. J., V. Lenschow, and U. Schwabe. Two affinity states of R_i adenosine receptors in brain membranes: analysis of guanine nucleotide and temperature effects on radioligand binding. *Mol. Pharmacol.* **28**:1–9 (1984).
18. Leung, E., and R. D. Green. Density gradient profiles of A_1 adenosine receptors labeled by agonist and antagonist radioligands before and after detergent solubilization. *Mol. Pharmacol.* **36**:412–419 (1989).
19. Stiles, G. L. The A_1 adenosine receptor: solubilization and characterization of a guanine nucleotide-sensitive form of the receptor. *J. Biol. Chem.* **260**:6728–6732 (1985).
20. Yeung, S.-M. H., E. Perez-Reyes, and D. M. F. Cooper. Hydrodynamic properties of adenosine receptors solubilized from rat cerebral-cortical membranes. *Biochem. J.* **248**:635–642 (1987).

21. Limbird, L. E., and R. J. Lefkowitz. Agonist-induced increase in apparent *beta*-adrenergic receptor size. *Proc. Natl. Acad. Sci. USA* **75**:228–232 (1978).
22. Smith, S. K., and L. E. Limbird. Solubilization of human platelet *alpha*-adrenergic receptors: evidence that agonist occupancy of the receptor stabilizes receptor-effector interactions. *Proc. Natl. Acad. Sci. USA* **78**:4026–4030 (1981).
23. Michel, T. B., B. Hoffman, R. J. Lefkowitz, and M. C. Caron. Different sedimentation properties of agonist- and antagonist-labeled platelet $alpha_2$ adrenergic receptors. *Biochem. Biophys. Res. Commun.* **100**:1131–1136 (1981).
24. Leung, E., M. M. Kwatra, M. M. Hosey, and R. D. Green. Characterization of cardiac A_1 adenosine receptors by ligand binding and photoaffinity labeling. *J. Pharmacol. Exp. Ther.* **244**:1150–1156 (1988).
25. Bruns, R. F., K. Lawson-Wendling, and T. A. Pugsley. A rapid filtration assay for soluble receptors using polyethylenimine-treated fibers. *Anal. Biochem.* **132**:74–81 (1983).
26. Munson, P. J., and D. Rodbard. LIGAND: a versatile computerized approach for characterization of ligand-binding systems. *Anal. Biochem.* **107**:220–239 (1980).
27. Goldstein, R. F., and E. Leung. EQUIL: simulation and data analysis of binding reactions with arbitrary chemical models. *Anal. Biochem.*, in press.
28. Limbird, L. E. *Cell Surface Receptors: A Short Course on Theory and Methods.* Martinus Nijhoff, Boston (1986).
29. De Lean, A., J. M. Stadel, and R. J. Lefkowitz. A ternary complex model explains the agonist-specific binding properties of the adenylate cyclase-coupled *beta*-adrenergic receptor. *J. Biol. Chem.* **255**:7108–7117 (1980).
30. Jacobs, S., and P. Cuatrecasas. The mobile receptor hypothesis and "cooperativity" of hormone binding: application to insulin. *Biochem. Biophys. Acta* **433**:482–495 (1976).
31. Abramson, S. N., P. McGonigle, and P. B. Molinoff. Evaluation of models for analysis of radioligand binding data. *Mol. Pharmacol.* **31**:103–111 (1987).
32. Wreggett, K. A., and A. De Lean. The ternary complex model: its properties and application to ligand interactions with the D_2-dopamine receptor of the anterior pituitary gland. *Mol. Pharmacol.* **26**:214–227 (1984).
33. Williams, M., M. F. Jarvis, M. A. Sills, J. W. Ferkany, and A. Braunwalder. Biochemical characterization of the antagonist actions of the xanthines, PAPCX (1,3-dipropyl-8(2-amino-4-chloro)phenylxanthine) and 8-PT (8-phenyltheophylline) at adenosine A_1 and A_2 receptors in rat brain tissue. *Biochem. Pharmacol.* **22**:4024–4027 (1987).
34. Nakata, H. A_1 adenosine receptor of rat testis membranes: purification and partial characterization. *J. Biol. Chem.* **265**:671–677 (1990).
35. Peralta, E. G., A. Askenazi, J. W. Winslow, D. H. Smith, J. Ramachandran, and D. J. Capon. Distinct primary structures, ligand-binding properties and tissue-specific expression of four human muscarinic acetylcholine receptors. *EMBO J.* **6**:3923–3929 (1987).
36. Munshi, R., and J. Linden. Copurification of A_1 adenosine receptors and guanine nucleotide binding proteins from bovine brain. *J. Biol. Chem.* **264**:14853–14859 (1989).
37. Linden, J., R. Munshi, M. L. Arroyo, and A. Patel. Characteristics of A_1 adenosine receptors and guanine nucleotide binding proteins copurified from bovine brain, in *Purines in Cellular Signaling: Targets for New Drugs* (K. A. Jacobson, J. W. Daly, and V. C. Manganiello, eds.). Springer, in press.
38. Elazar, Z., G. Siegel, and S. Fuchs. Association of two pertussis toxin-sensitive G-proteins with the D_2-dopamine receptor from bovine striatum. *EMBO J.* **8**:2353–2357 (1989).
39. Colquhoun, D. The relation between classical and cooperative models for drug action, in *Drug Receptors* (H. P. Rang, ed.). University Park Press, Baltimore, 149–181 (1973).
40. Ehlert, F. J. The relationship between muscarinic receptor occupancy and adenylate cyclase inhibition in the rabbit myocardium. *Mol. Pharmacol.* **28**:410–421 (1985).
41. Costa, T., and A. Herz. Antagonists with negative intrinsic activity at δ opioid receptors coupled to GTP-binding proteins. *Proc. Natl. Acad. Sci. USA* **86**:7321–7325 (1989).
42. Vannucci, S. J., C. M. Klim, L. S. Martin, and K. F. LaNoue. A_1-adenosine receptor-mediated inhibition of adipocyte adenylate cyclase and lipolysis in Zucker rats. *Am. J. Physiol.* **257**:E871–E878 (1989).

Send reprint requests to: Dr. Richard D. Green, Dept. of Pharmacology, M/C 868, University of Illinois at Chicago, P.O. Box 6998, Chicago, IL 60680.